Research Article | Vol. 27, No. 22 / 28 October 2019 / Optics Express 32609
Optics EXPRESS

Time resolved characterization of Fabry-Perot quantum cascade lasers for use in a broadband "white light" source

YOHAN YOON,[1] CHRISTOPHER A. KENDZIORA,[2,*] ROBERT FURSTENBERG,[2] CHRISTOPHER J. BRESHIKE,[2] SEOKMIN JEON,[3] ROBERT B. BALOW,[4] AND R. ANDREW MCGILL[2]

[1]*American Society for Engineering Education Postdoctoral Fellow (residing at NRL), Washington DC 20036, USA*
[2]*Naval Research Laboratory, Code 6365, 4555 Overlook Ave. SW, Washington DC 20375, USA*
[3]*National Research Council (NRC) Research Associateship Program (residing at NRL), Washington, DC 20375, USA*
[4]*Naval Research Laboratory, Code 6178, 4555 Overlook Ave. SW, Washington DC 20375, USA*
[*]*chris.kendziora@nrl.navy.mil*

Abstract: We report the time resolved characterization of Fabry-Perot quantum cascade lasers (FP-QCLs). We are developing a custom-built broadband laser source in the Mid-LWIR range by combining several high power FP-QCLs for a single snap shot application. This white light source would enable not only stand-off detection applications in a single snapshot but also new data collection modalities such as live, real-time chemical imaging, requiring extremely rapid measurements. In this study, the two FP-QCLs were operated in CW and pulsed modes with varying applied currents and diode temperatures to optimize the best laser operation condition to cover a broad spectral range including spectral features for the analytes of interest. To understand mode behavior of the FP-QCLs in a short period of time, the spectral output for each test condition was temporally resolved. Under most of the conditions, FP mode hopping was observed during the time evolution through the pulse length (3000 ns). Based on the time-resolved spectra, the ideal spectral characteristics for a single snap shot application are discussed, with respect to a broad spectral bandwidth, a flat-top power profile, and high spectral power density.

1. Introduction

Due to their high brightness and spectral range, quantum cascade lasers (QCLs) have been an attractive light source for several spectroscopic applications, including stand-off spectroscopy [1–5] and micro-spectroscopy [6,7]. For many spectroscopic applications, high spectral power density and broad spectral coverage are essential. A tunable external cavity QCL (EC-QCL) is a good candidate for those applications due to its high optical power density and broad wavelength coverage in the Mid-LWIR. However, beam wander induced by mode hops of the laser while the wavelength is tuned is a challenge [8–12]. While the wavelength is swept, a translation of the laser spot at the sample position can be induced by any fluctuation of the laser beam direction out of the cavity and beam profile. If unaccounted for, beam wander can lead to diminished performance (both in sensitivity and selectivity) for the spectroscopic technique.

Many types of QCLs, such as distributed feedback (DFB) QCLs [13–15] and optical frequency combs [16–18], have been used for spectroscopic applications. A Fabry-Perot QCL (FP-QCL) can be a good alternative laser source in the Mid-LWIR range due to the available high power density and broad spectral bandwidth [19,20]. In this work, we are developing a custom-built laser source by combining the output of multiple FP-QCLs on a single platform. Each of the FP-QCLs provides a unique spectral coverage. Due to the broad spectral coverage, this customized

#374887 https://doi.org/10.1364/OE.27.032609
Journal © 2019 Received 16 Aug 2019; revised 3 Oct 2019; accepted 4 Oct 2019; published 24 Oct 2019

Optics EXPRESS

"white" broadband FP-QCL array is an interesting light source to consider for spectroscopic stand-off detection in a single snapshot application. This single snap shot measurement using high power coherent FP-QCLs can be performed in a very short microsecond time scale, with no required wavelength tuning. This is enabling for the detection of chemical analytes on moving targets or from a moving platform or when both are moving. During QCL operation, the cavity temperature changes in a short time period, depending on drive currents and pulse duration, resulting in variances of spectral bandwidth and intensity profile [20,21]. Temporally resolved spectral information is required to help develop the combined broadband FP-QCL array for a single snapshot application. In this work, we characterize the time resolved spectral output in terms of spectral bandwidth, power profile, and output power density for two different FP-QCLs.

Unlike the wavelength tuning achieved using an external cavity QCL, a spectroscopic analysis technique is required for a single snapshot technique using a broadband "white" laser. In this regard, for future work, we plan to incorporate a spatial heterodyne spectrometer (SHS) to discriminate spectral and spatial information from single snapshot data [22,23].

2. Time-averaged characterization of FP-QCLs

We are currently developing a custom-built laser source by combining the output of multiple FP-QCLs on a single platform [24,25]. A schematic of the broadband FP-QCLs is shown in Fig. 1(a). The output of several high power FP-QCLs are combined to provide broad spectral coverage in the Mid-LWIR range. The FP-QCLs are electrically and thermally connected to copper blocks. The copper blocks with the FP-QCLs are mounted on a single metal support. The temperature of the FP-QCLs and copper blocks are controlled by thermoelectric coolers (TECs) between the copper blocks and the metal support. The TEC elements are operated by a temperature controller. Each FP-QCL is connected to a laser driver. The laser driver is connected to a function generator and a power supply so that the output of each FP-QCL is independently controlled.

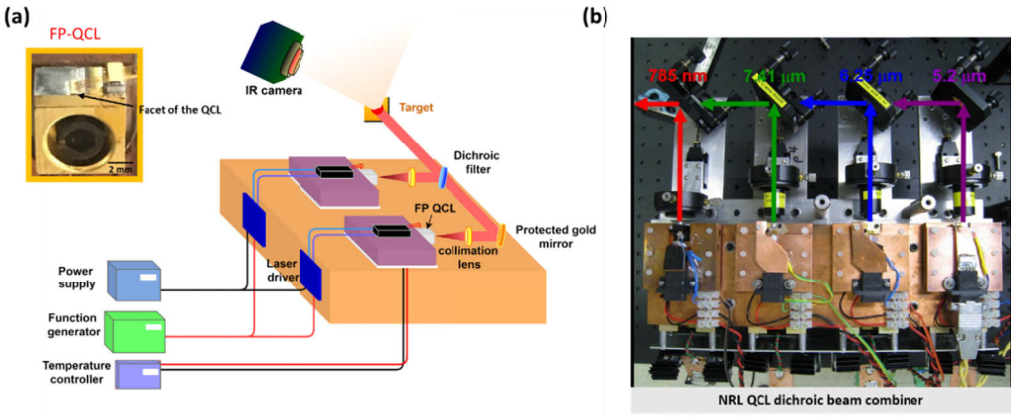

Fig. 1. A schematic of the broadband laser source. a) Two FP-QCLs are electrically and thermally connected to copper blocks. The copper blocks with FP-QCLs are mounted on a metal support. The temperature of FP QCLs and copper blocks are controlled by thermoelectric coolers (TECs) between the copper blocks and the metal support. The TEC elements are operated by a temperature controller. Each FP-QCL is connected to a laser driver. The output of the FP-QCLs are controlled by a power supply and a function generator connected to the laser driver. The output of the laser beams are collimated by ZnSe lenses and combined by dichroic filters. The combined beam illuminates the target and the diffusely reflected signal is collected by an IR camera. The inset shows an FP-QCL array mounted on a copper block. b) A photograph of the NRL QCL dichroic beam combiner.

Optics EXPRESS

The output beam can be operated either in a continuous wave (CW) mode or in a pulsed mode by implementing the function generator. The intensity of the laser beam is controlled by the power supply voltage. The output beams are collimated by ZnSe collimation lenses (12.7 mm focal length). The collimated laser beams are combined by dichroic filters and illuminate the surface of an Infragold disk. The diffusely reflected light is collected by an IR camera.

The electro-optical properties of high power FP-QCLs were characterized. Figure 2 shows representative I-V-P (current-voltage-optical power) curves for two commercially available FP-QCLs (QCL #1: AdTech CM7-25 and QCL #2: AdTech CM7-10-29) in CW mode. A FP-QCL emits a light cone at the front facet when a suitable current is applied. QCL #1, as shown in Fig. 2(a), starts emitting when 556 mA (threshold current) is applied at 15 °C, and optical output power dramatically increases by driving higher currents. Similarly, the light emission of QCL #2 starts when 532 mA is applied at 15 °C and the increase of optical output is observed at higher currents, see Fig. 2(b). In both QCLs, optical output curves as a function of current shift to the right at the higher temperature (22 °C), which requires higher currents to obtain the same optical output powers.

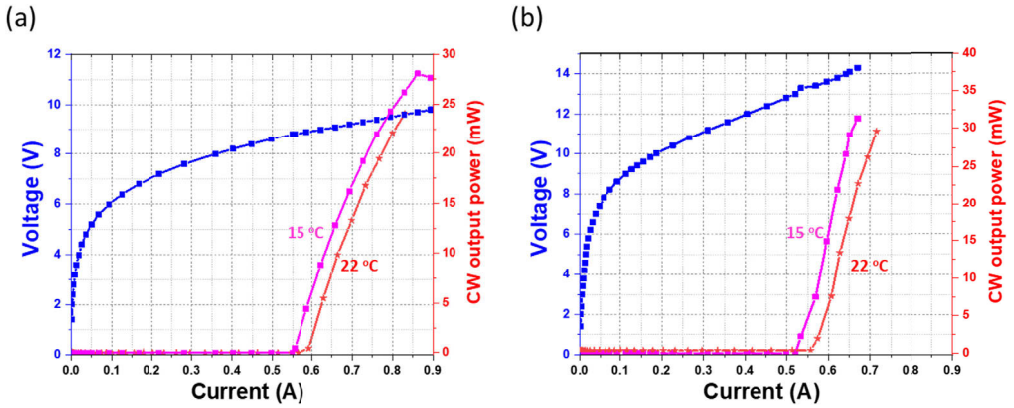

Fig. 2. Representative I-V-P curves for FP-QCLs (a) QCL #1 and (b) QCL #2. The blue line indicates applied voltages (left vertical axis) and the magenta (15 °C) and red (22 °C) lines represent laser optical powers (right vertical axis).

Figure 3 shows the time-averaged spectral output of QCL #1 operated in both CW and pulsed modes at a 15 °C diode temperature. The spectral outputs were collected using a Bruker Fourier transform infrared (FTIR) spectrometer with a resolution of 0.2 cm^{-1}. As shown in Fig. 3(a), an extremely narrow spontaneous emission ($\lambda = 7.35$ µm) is observed at the threshold current (556 mA). The emission spectrum is broadened by driving higher currents. When 891 mA is applied to QCL #1, a relatively broad emission spectrum is produced, covering the range from 7.25 µm to 7.55 µm. Figure 3(b) shows a representative emission spectrum for QCL #1 operated in pulsed mode (100 kHz repetition rate, 3000 ns pulse width, 30% duty cycle) at 15 °C. Like the CW mode, the emission spectra also broaden by driving higher currents. However, the spectral outputs in pulsed mode are different from those in CW mode in terms of spectral range, spectral profile, and output intensity. At low currents around the threshold current (556 mA), the spectral bandwidths in pulsed mode are wider than those in CW mode. By driving pulses at higher currents, the spectral bandwidths are similar to those observed in CW, even though the spectral coverages are slightly shifted. To minimize temperature variation or reduce the thermal load while the FP-QCL emits at high currents, the FP-QCL can be operated in pulsed mode. In the rest of this paper, we focus upon the spectral output of FP-QCLs in pulsed mode.

Optics EXPRESS

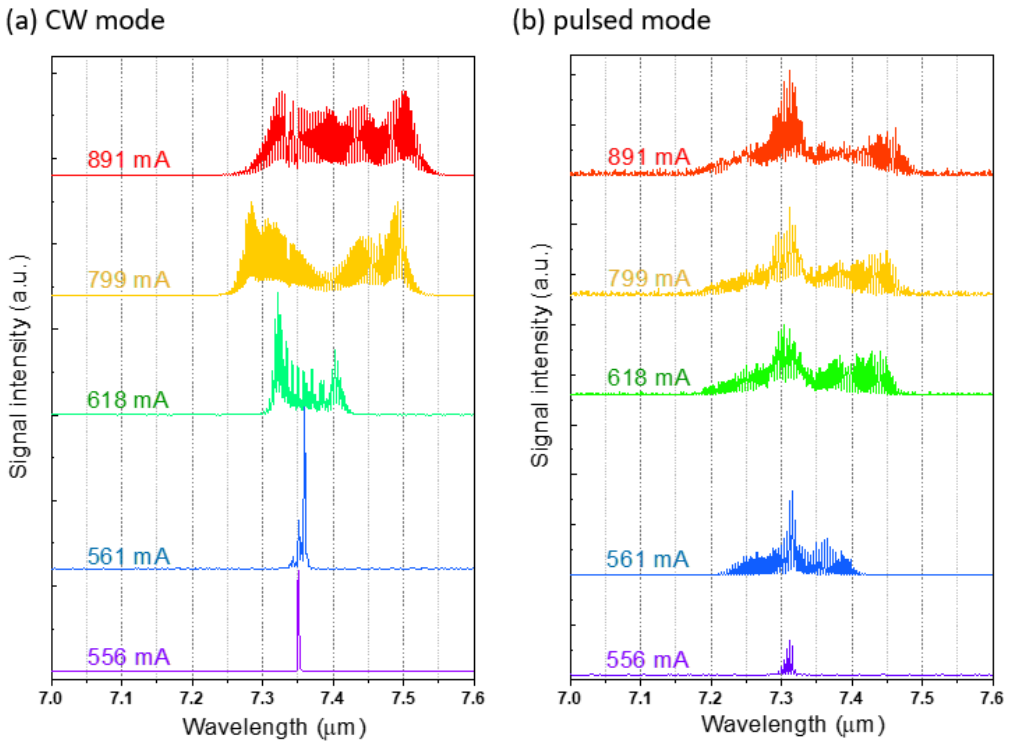

Fig. 3. Emission spectra from QCL #1 operated in (a) CW mode and (b) pulsed mode. The spectra were collected using a Bruker FTIR spectrometer. The diode temperature is 15 °C. The pulse repetition rate is 100 kHz and pulse width is 3000 ns.

3. Time-resolved characterization of FP-QCLs

The time-averaged spectra shown in Fig. 3 were acquired by accumulating all spectral features while the FTIR spectra were collected, typically over a few seconds. This information would be useful to most spectroscopic applications, which do not require nano-second or micro-second time resolutions. However, for a single snap shot spectroscopy, it is critical to resolve temporal information during the voltage pulse duration time. For most applications using this light source, the averaged spectrum is all that matters when pulse duration time is shorter than the camera acquisition time. However, if pulse duration time is longer than the camera acquisition time, time-resolved measurements are very helpful to understand how to best pick the optimal laser pulse parameters that yield the spectrally flattest averaged spectrum, as is shown in this paper. Time resolved spectral (TRS) measurements were performed in step scan mode using a Bruker Vertex 70v FTIR spectrometer. A fast (1 ns rise time) HgCdTe detector (Daylight Solutions, HPC-2TE-100) was used to monitor the laser output. A fast transient recorder (Spectrum instrumentation, M3i.4142 EXP) was used to record signals from the detector. The sampling rate used was 400 MS/s, and time resolution was 2.5 ns. The voltage pulser (function generator) connected to the FP-QCLs was used as a trigger source for the transient recorder. The spectral resolution of the step scan mode was 1 cm^{-1}. The total acquisition time for a step scan is about 25 min. To minimize the total acquisition time, a relatively low spectral resolution was selected. Figure 4 shows contour maps of temporally resolved spectra of QCL #1 with 6 different applied currents from 556 mA to 952 mA. The pulse repetition rate was 100 kHz and pulse width was 3000 ns. The diode temperature was 15 °C.

Optics EXPRESS

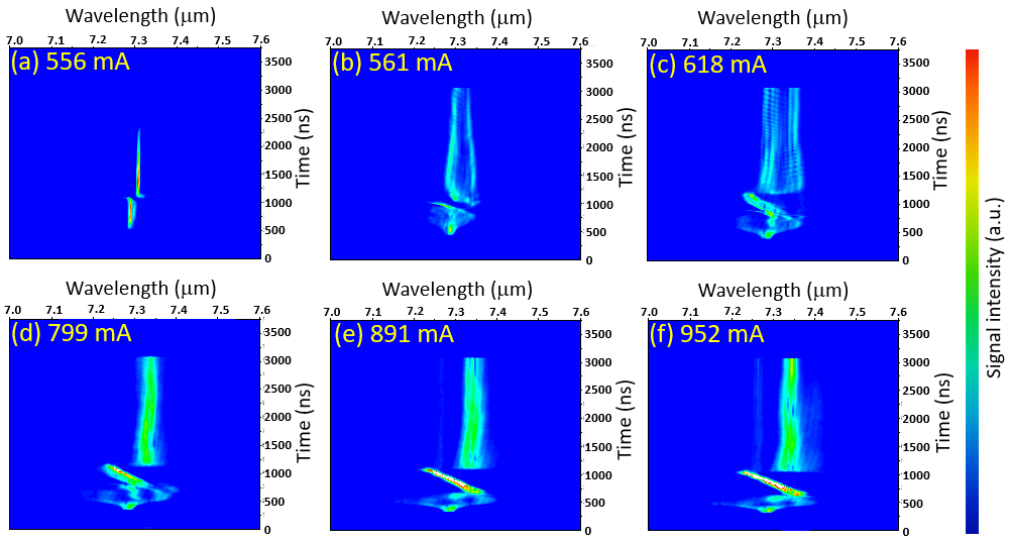

Fig. 4. Contour maps of time resolved spectra of the FP-QCL #1 with 6 different applied currents from 556 mA to 952 mA. The pulse repetition rate is 100 kHz and pulse width is 3000 ns. The diode temperature is 15 °C.

In the context of FP-QCLs, lateral modes are stable modes of oscillation involving light waves that are not propagating parallel to the laser cavity axis. In contrast, longitudinal modes of a resonant cavity are particular standing wave patterns formed by waves confined in the cavity. In this study, narrow spectral features with approximately 0.004 μm (0.75 cm^{-1}) are due to longitudinal modes and relatively broad spectral features seen in Fig. 4 are due to lateral FP modes of the cavity [20]. Due to the relatively low spectral resolution (1 cm^{-1}) of the step scan mode employed in this study, the longitudinal mode spacing is rarely resolved. However, in time averaged FTIR spectra performed with a 0.2 cm^{-1} spectral resolution (5 times higher spectral resolution than the step scan mode), longitudinal modes are observed more clearly as shown in Fig. 3(b). Each FP-QCL exhibits very different spectral output in terms of FP modes as well as spectral bandwidth, spectral profile, and power intensity. This spectral output information results from the properties of each QCL, such as materials and cavity properties. On the several hundred nano-second time scale (pulse duration time) for spectroscopic applications, the spectral output averaged over the pulse duration time significantly changes depending on mode hoppings. Therefore, time resolved measurements should be performed for each QCL for optimization of lasing parameters prior to its use as an illumination source.

As shown in Fig. 4(a), when the threshold current (556 mA) was applied, one dominant peak appears at 7.289 μm after a time delay of approximately 550 ns. Within the first 1110 ns, the peak is broadened in the wavelength range of 7.282 μm to 7.307 μm. After 1110 ns, a change of the lateral FP mode for QCL #1 is observed. The first lateral FP mode peak disappears and the second lateral FP mode emission is observed. The second lateral mode peak only lasts to 2280 ns. Because 2280 ns is shorter than the pulse width (3000 ns), this indicates that a further rise in the QCL temperature has caused the lasing to stop. At 561 mA, as shown in Fig. 4(b), a similar lateral FP mode distribution in the time evolution is also observed. However, the spectral output broadens to span from 7.258 μm to 7.331 μm. This second lateral mode is well established and lasts for the pulse duration time (3000 ns). A broader spectral output, spanning the pulse duration time, is observed by driving a higher current of 618 mA. Interestingly, a strong lateral shift of the spectral output (7.373 μm to 7.229 μm) is observed from 760 ns to 1207 ns. This lateral

Optics EXPRESS

mode hopping is seen more clearly when applying higher currents, as shown in Figs. 4(d)–4(f). At 799 mA, the intensity of the third lateral FP mode at 1145 ns is stronger and the spectral output is narrower when compared to spectra observed when applying 618 mA. This lateral mode is well established and lasts for the pulse duration time (3000 ns). At 891 mA and 952 mA, as shown in Figs. 4(e) and 4(f), similar mode changes and spectral output are observed, with slight broadening of the spectral outputs. Mode hopping is a phenomenon that occurs, when a laser operates in one resonator mode and then quickly switches to another mode, driven by some external influence such as heat. Mode hopping was not intentionally designed into these lasers because hopping makes it difficult to obtain continuous wavelength tuning. The variation of refractive index and thermal expansion of the Fabry-Perot resonator (cavity) with temperature can cause the wavelength shift. Also, inhomogeneity and dynamics of heating inside of the FP-QCL during the time it emits light can cause mode hopping and multimode lasing [10,26].

To observe the FP mode hopping behavior and FP mode lateral shift more clearly, individual time resolved spectra are extracted from the contour maps shown in Fig. 4. Figure 5 shows a representative series of temporally resolved spectra extracted from the contour map when 952 mA was applied to QCL #1, as shown in Fig. 4(f). The first lateral mode is initiated in the wavelength range of 7.261μm to 7.306 μm at 317 ns after the pulse starts. The first peak broadens and then disappears at 625 ns. At that moment, a new FP lateral mode appears and shifts to a lower wavelength of 7.202 μm. The third lateral FP mode consists of one strong peak, in the range of 7.304 μm to 7.369 μm, and a smaller peak around 7.246 μm to 7.292 μm appears at 1125 ns. The third lateral FP mode, lasts for the duration of the pulse. Longitudinal FP modes created in the laser cavity, as well as lateral FP modes are also observed, for example at 750 ns, 1125 ns, 1875 ns, and 2250 ns.

Figure 6 shows time resolved spectral outputs of QCL #1 when 952 mA is applied at three different diode temperatures (15 °C, 17 °C, and 19 °C). The temperature of QCL #1 is controlled by thermoelectric coolers (TECs) between the metal support and the copper block, which is interfaced to the QCL, as shown in Fig. 1(a). The TECs are controlled using a temperature controller. Figure 6(a) shows three representative spectral outputs extracted from the three contour maps (contour maps for 17 °C and 19 °C are not shown) at 2625 ns. Figure 6(b) shows time resolved spectral output on a finer wavelength scale. This graph clearly shows the red shift of the longitudinal FP modes with increasing QCL diode temperatures. The peak positions of the longitudinal mode are 7.2547 μm, 7.2562 μm, and 7.2575 μm at 15 °C, 17 °C, and 19 °C, respectively. The red shift of the mode from 15 °C to 19 °C is 0.0028 μm (0.532 cm^{-1}). The shift of the FP modes is mainly due to the variation of refractive index and the thermal expansion of the Fabry-Perot resonator (cavity) with temperature.

Figure 7 shows a series of time resolved spectral outputs for QCL #1 shown earlier in Fig. 5. This is a stack of spectral outputs at 13 different time steps for the pulse duration time from 317 ns to 3000 ns. The pulse repetition rate is 100 kHz and pulse width is 3000 ns. The diode temperature is 15 °C and the applied current is 952 mA. As shown in Fig. 7(a), the spectral output of the QCL is in the wavelength range of 7.1361 μm to 7.4541 μm with a bandwidth of 0.318 μm (59.782 cm^{-1}). For comparison with the time resolved spectra, we performed a conventional time-averaged FTIR measurement for QCL #1, as shown in Fig. 7(b). The QCL was also operated in pulsed mode with the same conditions for the time averaged measurements as for the time resolved step scan measurements. The spectral resolution used in these measurements was 1 cm^{-1}. The time averaged spectral output contains all accumulated spectral features while the spectrum was collected, which took several seconds (32 scan averaging). Therefore, the conventional FTIR spectrum contains all the spectral information of the contour map shown in Fig. 4(f), averaged over many pulses. Note that the time-resolved spectra, representing spectral information on a short period scale, shown in Fig. 7(a), are essential for a single snap shot application.

Optics EXPRESS

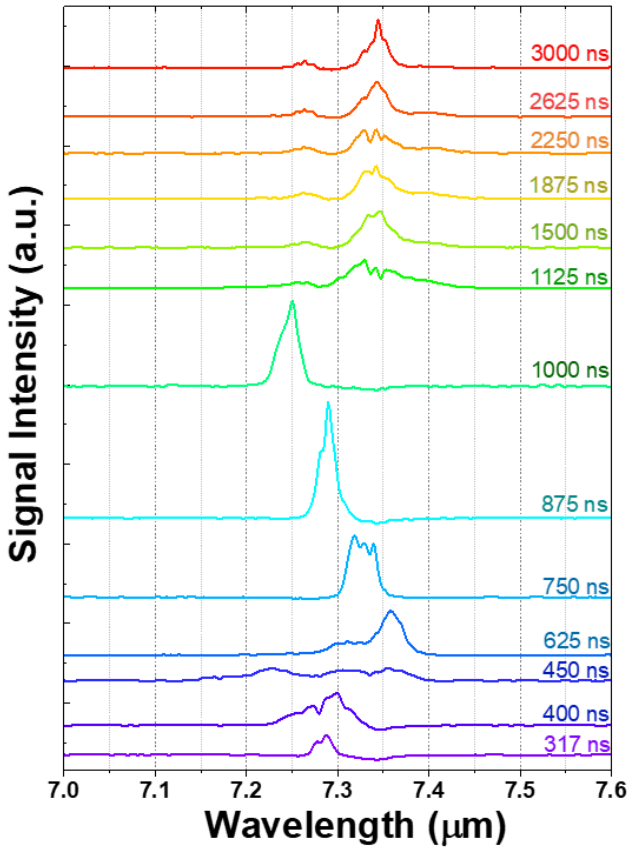

Fig. 5. Time resolved spectral output extracted from the contour maps in Fig. 4. The graph shows spectral outputs with 13 different time values from 317 ns to 3000 ns. The pulse repetition rate is 100 kHz and pulse width is 3000 ns. The diode temperature is 15 °C. Applied current is 952 mA.

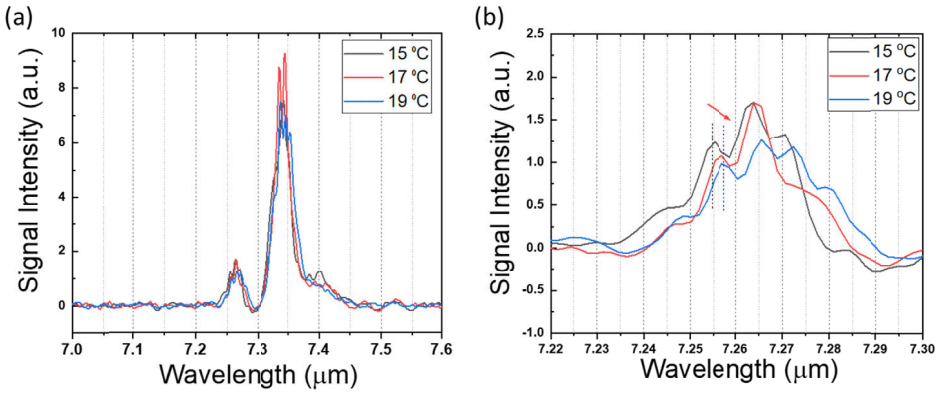

Fig. 6. (a) Time resolved spectral outputs of the QCL #1 operated in pulsed mode with three different diode temperatures (15 °C, 17 °C, and 19 °C). (b) Finer wavelength scale representation of the time resolved spectral output with various diode temperatures. The pulse repetition rate is 100 kHz and pulse width is 3000 ns. Applied current is 952 mA.

Optics EXPRESS

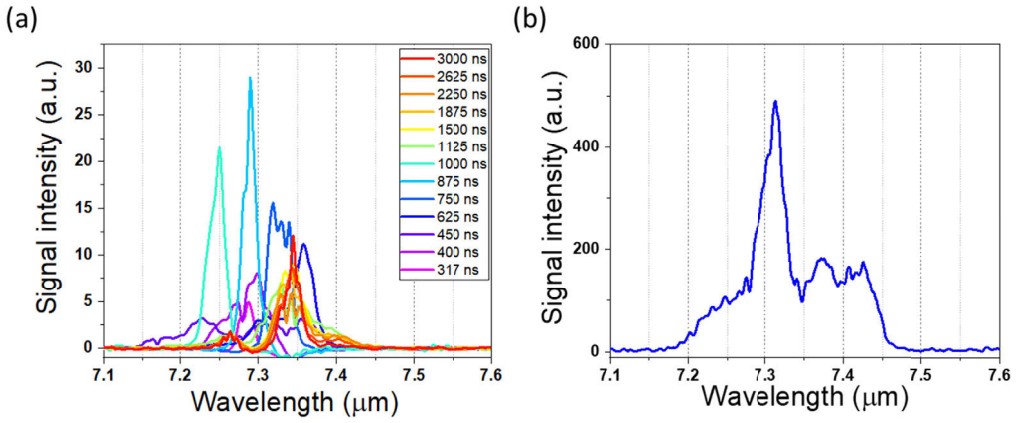

Fig. 7. (a) Series of time resolved spectral outputs of QCL #1 operated in pulsed mode. The pulse repetition rate is 100 kHz and pulse width is 3000 ns. The diode temperature is 15 °C and the applied current is 952 mA. (b) Non-time resolved conventional FTIR spectrum for the QCL#1 operated in pulsed mode.

Figure 8 shows contour maps of time resolved spectral outputs for another FP-QCL (QCL #2) with 6 different applied currents from 532 mA to 678 mA. The pulse repetition rate is 100 kHz and pulse width is 3000 ns. The diode temperature is 15 °C. A spontaneous emission at 5.254 μm at the threshold current (532 mA) is extremely sharp in terms of wavelength, as shown in Fig. 8(a). This first FP lateral mode disappears at 845 ns after the voltage pulse starts. This first lateral mode becomes stronger and lasts for the duration of the pulse when the current increases to 598 mA, as shown in Fig. 8(c). When 629 mA is applied to QCL #2, the spectral output becomes broadened and the first lateral FP mode is separated into a multi-lateral mode, see Fig. 8(d). The bandwidth of the spectral output becomes wider when a higher current is applied. When 678 mA is applied, Fig. 8(f) shows a spectral output across the wavelength range from 5.161 μm to 5.314 μm with a 0.153 μm (55.787 cm^{-1}) spectral breadth. The second lateral FP mode lasts for the pulse duration time.

To examine the influence of each parameter, i.e. current, time, and wavelength, on the light emission of the QCL #2, multiple spectral outputs were extracted from the contour maps shown in Fig. 8. Figure 9(a) shows the current-dependent spectral outputs as a function of wavelength. The graph shows the QCL #2 output signal at 700 ns after the pulse starts with 6 different applied currents. At the threshold current of 532 mA, a spontaneous emission observed at 5.254 μm is extremely sharp but weak. The peak becomes broadened and stronger by driving at higher currents and has a spectral output bandwidth in the wavelength range of 5.146 μm to 5.328 μm when 678 mA is applied. Time resolved spectral outputs when 678 mA is applied are shown in Fig. 9(b). The initial spectral output at 305 ns after the pulse starts is already quite strong and wide, when compared to the initial output at the threshold current (532 mA). As shown in Fig. 8, the first lateral FP mode broadens into a second lateral FP mode at around 500 ns after the pulse starts. The spectral bandwidth and signal intensity of the two lateral FP modes do not significantly change and persist for the rest of the pulse duration time. The multiple longitudinal FP modes are also seen as spikes in each spectral output. The longitudinal FP mode at 5.3 μm appears in the second lateral FP mode and disappears at 2750 ns. The evolution of the FP modes is clearly seen in the wavelength dependent time resolved spectral output shown in Fig. 9(c). This graph shows the signal intensity change as a function of time at 3 different wavelengths (5.194 μm, 5.255 μm, and 5.279 μm) when 678 mA is applied. The longitudinal FP mode at 5.255 μm (red line in the graph) is initiated at around 305 ns and becomes weaker in the

Optics EXPRESS

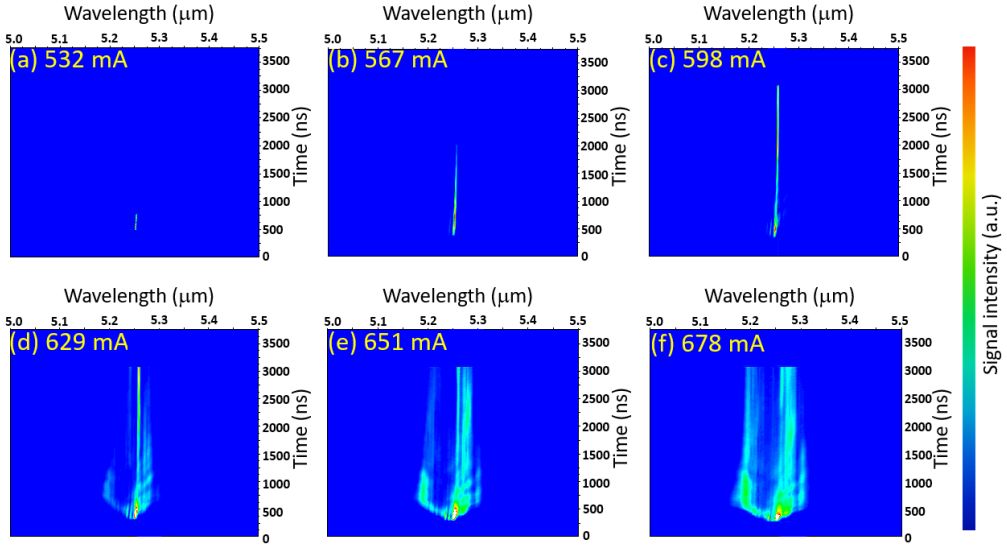

Fig. 8. Contour maps of time resolved spectra of QCL #2 with 6 different applied currents from 532 mA to 678 mA. The pulse repetition rate is 100 kHz and pulse width is 3000 ns. The diode temperature is 15 °C.

time evolution. The peak totally disappears after 2000ns. Two other representative longitudinal FP modes at 5.194 μm and 5.279 μm appear when the second lateral FP mode is initiated and saturated after some fluctuation. These modes last for the rest of the pulse duration time.

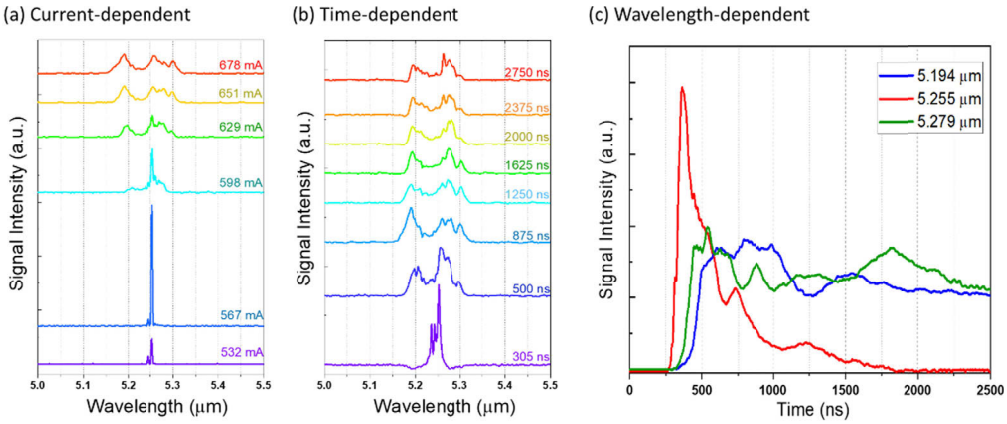

Fig. 9. Spectral output extracted from the contour maps in Fig. 8. The graph shows the influence of each parameter, e.g. current, time, wavelength, on the signal from QCL #2. (a) Current-dependent signal as a function of wavelength at 700 ns after the pulse starts with 6 different currents from 532 mA to 678 mA. (b) Time-dependent signal as a function of wavelength with 8 different time scales from 305 ns to 2750 ns when 678 mA is applied. (c) Wavelength-dependent signal as a function of time with 3 different wavelengths (5.194 μm, 5.255 μm, and 5.279 μm) when 678 mA is applied. The pulse repetition rate is 100 kHz and pulse width is 3000 ns. The diode temperature is 15 °C.

Optics EXPRESS

4. Discussion

In this work, time resolved characterization for a custom-built broadband laser source in the Mid-LWIR range was studied. This "white" broadband laser source can simultaneously excite a wide range of absorption bands present in a variety of chemical analytes. This enables the white source to be used in stand-off detection applications in a single snapshot, and a variety of other spectroscopic techniques, for extremely rapid measurements, including those where the target or light source or both are in motion during a measurement. Since the single snap shot should be performed in a very short time period, temporally resolved spectral information must be acquired prior to employing the light source in a spectroscopic application. For a successful spectroscopic application, several conditions need to be optimized.

First, the spectral coverage of the combined FP-QCLs should be as broad as possible to adequately cover the spectral features for the analytes of interest. If the spectral bandwidth of the combined FP-QCLs is relatively narrow, the number of spectral features that can be detected in a single snap shot is limited. As shown in the contour maps of time resolved spectra of the FP-QCLs, Fig. 4 and Fig. 8, the spectral output bandwidth varies with applied current and time. In addition, changes in the diode temperature result in spectral output shifts of the QCLs. In this study, we are aiming to determine the optimum operating conditions for the QCLs to achieve the broadest spectral output, as investigated through temporally resolved spectra. The broadest spectral output in the contour map of time resolved spectra for QCL #1, shown in Fig. 4, is observed at 470 ns after 952 mA is applied. The spectral output is in the wavelength range of 7.151 μm to 7.411 μm. The maximum spectral bandwidth of QCL #2 is acquired at 575 ns after 678 mA is applied. The range of spectral output is from 5.161 μm to 5.314 μm.

Second, the optical power output of the FP-QCLs should ideally be evenly distributed over the full operating spectral range. While the spectral output broadens by driving at higher currents, the spectrum profile also changes. A smooth flat-top spectrum is ideal for spectroscopic applications. However, a perfect flat-top spectrum does not exist at any time through the evolution. The most flat-top spectrum for QCL #1 in Fig. 5 is observed at 450 ns after 952 mA is applied. Asymmetric profile shapes of temporally resolved spectra are observed for the rest of the time through the evolution. In the time resolved spectra of QCL #2, a flat-top spectrum is rarely achieved since the initial spectral output quickly splits into two modes, resulting in two distinct peaks, as seen in Fig. 8. The optimum spectrum achieved was at 1250 ns after 678 mA is applied, as seen in Fig. 9(b).

Third, each wavelength should have enough spectral output density for the intended application. Even where broad bandwidth, stable, and flat-top spectra are obtained, the weak scattering signal from a trace explosives target, in a standoff detection application, will require enough spectral power density to discriminate spectral features of analytes. The spectral output at 450 ns after a 952 mA is applied, as shown in Fig. 5, exhibits a relatively smooth and flat-top profile. However, the spectral power density at each wavelength is lower than for some other conditions. Therefore, the laser output at this condition might not offer optimal spectral power density for spectroscopic applications.

Overall, the three properties of spectral output: 1) broad spectral width, 2) flat-top, and 3) high spectral power density, described above are desirable features when FP-QCLs are being considered for use in a broadband "white" laser source for single snap shot applications. Mostly, there exists a trade-off between these properties. As shown in the current-dependent and time-dependent spectra in Figs. 9(a) and 9(b), spectral bandwidth is normally in inverse correlation with spectral output density. As the spectra broaden, spectral density at each wavelength drops. In this study, we demonstrate that the spectral profile and power density of the FP-QCLs change with operating conditions and time. In addition, the spectral output varies between FP-QCLs, with each chip exhibiting unique characteristics, although common trends are observed across QCLs.

Optics EXPRESS

5. Conclusion

In summary, we are developing a custom-built broadband laser source by combining several high power FP-QCLs to achieve broad spectral coverage in the Mid-LWIR range. Each of the FP-QCLs was connected to a laser driver so that the FP-QCL was independently controlled. The QCLs were operated in either CW or pulsed mode. The spectral outputs were characterized using a Bruker FTIR spectrometer. For time resolved measurements, the two different FP-QCLs were operated in pulsed mode, and the output spectra were collected with several pulse currents and diode temperatures in a step scan mode of the FTIR spectrometer. For QCL #1, the peak becomes broadened and stronger by driving higher currents. In the time resolved spectra, a strong lateral FP mode distribution is observed in the first 317 ns of the time evolution. The first peak broadens and then disappears at 625 ns. At that moment, a new FP lateral mode appears and shifts to a lower wavelength of 7.202 μm. The third FP lateral mode appears at 1125 ns and lasts for the pulse duration time (3000 ns). By increasing diode temperature, the spectra observed exhibit a red shift for the longitudinal FP modes. A different FP mode hopping behavior was observed for the QCL #2. After a certain current (629 mA) is applied to the QCL, the spectral output becomes broadened and the first lateral FP mode is seUnitparated into a second lateral mode consisting of two distinct peaks. The spectra become stronger in the wavelength range of 5.161 μm to 5.314 μm with 0.153 μm (55.787 cm^{-1}) spectral bandwidth, when 678 mA is applied. The second lateral FP mode lasts for the pulse duration time. In this work, we have experimentally demonstrated FP mode hopping for two different FP-QCLs and the spectral output change in terms of spectral width, profile shape and spectral power density, which affect the performance of the FP-QCLs. Temporally resolved characterization of the different FP-QCLs used in this work provides useful spectral information, especially for single snap shot application.

Funding

Office of Naval Research/ U.S. Naval Research Laboratory base program (Work Unit 1C33).

References

1. C. A. Kendziora, R. Furstenberg, M. Papantonakis, V. Nguyen, J. Byers, and R. A. McGill, "Infrared photothermal imaging spectroscopy for detection of trace explosives on surfaces," Appl. Opt. **54**(31), F129–F138 (2015).
2. R. Furstenberg, C. A. Kendziora, J. Stepnowski, S. V. Stepnowski, M. Rake, M. R. Papantonakis, V. Nguyen, G. K. Hubler, and R. A. McGill, "Stand-off detection of trace explosives via resonant infrared photothermal imaging," Appl. Phys. Lett. **93**(22), 224103 (2008).
3. F. Fuchs, B. Hinkov, S. Hugger, J. M. Kaster, R. Aidam, W. Bronner, K. Köhler, Q. Yang, S. Rademacher, K. Degreif, F. Schnürer, and W. Schweikert, "Imaging stand-off detection of explosives using tunable MIR quantum cascade lasers," Proc. SPIE **7608**, 760809 (2010).
4. M. F. Witinski, R. Blanchard, C. Pfluegl, L. Diehl, B. Li, K. Krishnamurthy, B. C. Pein, M. Azimi, P. Chen, G. Ulu, G. Vander Rhodes, C. R. Howle, L. Lee, R. J. Clewes, B. Williams, and D. Vakhshoori, "Portable standoff spectrometer for hazard identification using integrated quantum cascade laser arrays from 6.5 to 11 μm," Opt. Express **26**(9), 12159–12168 (2018).
5. C. J. Breshike, C. A. Kendziora, R. Furstenberg, V. Nguyen, A. Kusterbeck, and R. Andrew McGill, "Infrared backscatter imaging spectroscopy of trace analytes at standoff," J. Appl. Phys. **125**(10), 104901 (2019).
6. R. Furstenberg, C. A. Kendziora, M. R. Papantonakis, V. Nguyen, and R. A. McGill, "Chemical imaging using infrared photothermal microspectroscopy," Proc. SPIE **8374**, 837411 (2012).
7. A. Hasenkampf, N. Kröger, A. Schönhals, W. Petrich, and A. Pucci, "Surface-enhanced mid-infrared spectroscopy using a quantum cascade laser," Opt. Express **23**(5), 5670–5680 (2015).
8. C. J. Breshike, C. A. Kendziora, R. Furstenberg, V. Nguyen, and R. A. McGill, "Stabilizing infrared quantum cascade laser beams for standoff detection applications.," Proc. SPIE **10111**, 10111B (2017).
9. R. Müller, C. A. Kendziora, and R. Furstenberg, "Feedback stabilization of quantum cascade laser beams for stand-off applications," Proc. SPIE **10194**, 101942U (2017).
10. R. Furstenberg, C. A. Kendziora, M. R. Papantonakis, V. Nguyen, and R. A. McGill, "Characterization and control of tunable quantum cascade laser beam parameters for stand-off spectroscopy," Proc. SPIE **9824**, 98240L (2016).
11. Y. Yoon, C. J. Breshike, C. A. Kendziora, R. Furstenberg, and R. Andrew McGill, "Reduction of speckle noise and mitigation of beam wander in tunable external cavity quantum cascade lasers using rotating diamond/KBr pellet coupled with multimode fiber," Opt. Express **27**(6), 8011–8020 (2019).

Optics EXPRESS

12. Y. Yoon, C. J. Breshike, C. A. Kendziora, R. Furstenberg, and R. Andrew McGill, "Control of quantum cascade laser sources in stand-off detection of trace explosives," Proc. SPIE **10983**, 109830G (2019).
13. H.-W. Hubers, S. G. Pavlov, H. Richter, A. D. Semenov, L. Mahler, A. Tredicucci, H. E. Beere, and D. A. Ritchie, "High-resolution gas phase spectroscopy with a distributed feedback terahertz quantum cascade laser," Appl. Phys. Lett. **89**(6), 061115 (2006).
14. B. G. Lee, M. A. Belkin, R. Audet, J. MacArthur, L. Diehl, C. Pflügl, F. Capasso, D. C. Oakley, D. Chapman, A. Napoleone, D. Bour, S. Corzine, G. Höfler, and J. Faist, "Widely tunable single-mode quantum cascade laser source for mid-infrared spectroscopy," Appl. Phys. Lett. **91**(23), 231101 (2007).
15. A. Castrillo, E. De Tommasi, L. Gianfrani, L. Sirigu, and J. Faist, "Doppler-free saturated-absorption spectroscopy of CO2 at 4.3 microm by means of a distributed feedback quantum cascade laser," Opt. Lett. **31**(20), 3040–3042 (2006).
16. G. Villares, A. Hugi, S. Blaser, and J. Faist, "Dual-comb spectroscopy based on quantum-cascade-laser frequency combs," Nat. Commun. **5**(1), 5192 (2014).
17. S. Bartalini, L. Consolino, P. Cancio, P. De Natale, P. Bartolini, A. Taschin, M. De Pas, H. Beere, D. A. Ritchie, M. S. Vitiello, and R. Torre, "Frequency-comb-assisted terahertz quantum cascade laser spectroscopy," Phys. Rev. X **4**(2), 021006 (2014).
18. I. Galli, S. Bartalini, P. Cancio, F. Cappelli, G. Giusfredi, D. Mazzotti, N. Akikusa, M. Yamanishi, and P. De Natale, "Mid-infrared frequency comb for broadband high precision and sensitivity molecular spectroscopy," Opt. Lett. **39**(17), 5050 (2014).
19. Y. Wang, M. G. Soskind, W. Wang, and G. Wysocki, "High-resolution multi-heterodyne spectroscopy based on Fabry-Perot quantum cascade lasers," Appl. Phys. Lett. **104**(3), 031114 (2014).
20. S. Gundogdu, H. S. Pisheh, A. Demir, M. Gunoven, A. Aydinli, and C. Sirtori, "Time resolved Fabry-Perot measurements of cavity temperature in pulsed QCLs," Opt. Express **26**(6), 6572–6580 (2018).
21. B. Hinkov, Q. Yang, F. Fuchs, W. Bronner, K. Köhler, and J. Wagner, "Time-resolved characterization of external-cavity quantum-cascade lasers," Appl. Phys. Lett. **94**(22), 221105 (2009).
22. C. R. Englert, J. M. Harlander, C. M. Brown, and K. D. Marr, "Spatial heterodyne spectroscopy at the Naval Research Laboratory," Appl. Opt. **54**(31), F158–F163 (2015).
23. C. R. Englert, D. D. Babcock, and J. M. Harlander, "Spatial heterodyne spectroscopy for long-wave infrared: First measurements of broadband spectra," Opt. Eng. **48**(10), 105602 (2009).
24. C. A. Kendziora, R. Furstenberg, M. Papantonakis, V. Nguyen, J. Stepnowski, and R. A. McGill, "Advances in stand-off detection of trace explosives by infrared photo-thermal imaging," Proc. SPIE **7664**, 76641J (2010).
25. R. Furstenberg, C. Kendziora, M. Papantonakis, S. V. Stepnowski, J. Stepnowski, V. Nguyen, M. Rake, and R. A. McGill, "Standoff detection of trace explosives by infrared photo-thermal spectroscopy," in *Proceedings of IEEE Conference on Technologies for Homeland Security (HST)* (IEEE, 2009), pp. 465–471.
26. R. Paschotta, *Encyclopedia of Laser Physics and Technology*, 1st ed. (Wiley-VCH, 2008).